PLOS ONE

RESEARCH ARTICLE

Sodium butyrate is incorporated into central metabolism in fly head while inducing oxygen consumption increase

Annika Müller-Eigner[1], Benedikt Gille[1], Frederik Dethloff[2], Chen Meng[3], Christina Ludwig[3], John T. Heiker[4], Patrick Giavalisco[2], Shahaf Peleg[1]*

1 Research Group Energy Metabolism and Epigenetics, Research Institute for Farm Animal Biology (FBN), Dummerstorf, Germany, **2** Max Planck Institute for Biology of Ageing, Cologne, Germany, **3** Bavarian Center for Biomolecular Mass Spectrometry (BayBioMS), School of Life Sciences, Technical University of Munich, Freising, Germany, **4** Helmholtz Institute for Metabolic, Obesity and Vascular Research (HI-MAG) of the Helmholtz Zentrum München at the University of Leipzig and University Hospital Leipzig, Leipzig, Germany

* peleg@fbn-dummerstorf.de

Citation: Müller-Eigner A, Gille B, Dethloff F, Meng C, Ludwig C, Heiker JT, et al. (2024) Sodium butyrate is incorporated into central metabolism in fly head while inducing oxygen consumption increase. PLoS ONE 19(12): e0315892. https://doi.org/10.1371/journal.pone.0315892

Editor: Eugenio Llorens, Universitat Jaume 1, SPAIN

Received: July 31, 2024

Accepted: December 3, 2024

Published: December 19, 2024

Data Availability Statement: The mass spectrometric raw files as well as the MaxQuant output files have been deposited to the ProteomeXchange Consortium via the PRIDE partner repository and can be accessed using the identifier PXD050591 (https://proteomecentral.proteomexchange.org/cgi/GetDataset?ID=PXD050591, reviewer account username: reviewer_pxd050591@ebi.ac.uk, password: SMEZOwcq).

Abstract

Butyrate has been proposed as a drug therapy by acting as a lysine deacetylase (KDAC) inhibitor and elevating protein acetylation, in particular on histones. Nonetheless, recent studies suggest that tissues such as the gut can utilize butyrate as a metabolite. We have previously shown that the addition of butyrate induces a rapid increase of oxygen consumption in whole *Drosophila melanogaster* heads. Here we show that while head oxygen consumption is increased by the addition of butyrate, no apparent changes are observed on the proteome and acetylome. Instead, we show that butyrate is metabolized and incorporated into the tricarboxylic acid (TCA) cycle. Collectively our data supports the notion that the therapeutic benefits of acute butyrate treatment may be also mediated by improving metabolic rates, rather than solely targeting the epigenome or acetylome.

Introduction

Chromatin remodeling is a key mechanism, which enables living cells to react and adjust to changes in the environment. One core mechanism to modulate the chromatin is the modification of histones, a set of proteins that tightly interacts and packages the DNA [1–3]. Modification of histones by small metabolites lead to alterations in the binding between histone and DNA, resulting in fine-tuning of transcription [4, 5]. One of the most studied modifications of histone proteins is histone acetylation, which is commonly associated with reduced histone-DNA interaction that leads to increased transcription activity [6–9].

Dysregulation of chromatin remodeling during disease and aging has attracted considerable attention in the recent two decades. For example, the observation that histone acetylation levels are altered during aging and maladies such as neurodegeneration and Alzheimer's disease has led to identifying histone acetylation as an important target [10]. Indeed, the inhibition of histone deacetylases (HDACs) by drugs such as suberoylanilide hydroxamic acid (SAHA), butyrate and others has been shown to improve age-associated memory formation

Funding: SP lab is supported by the FBN, DFG grant (458246576), and by two Longevity Impetus grants from Norn Group and by a Longevity Impetus Grant from Norn Group, Hevolution Foundation and Rosenkranz Foundation. BG has been supported by a Longevity Impetus grant from Norn Group. JTH is supported by the DFG CRC1052 (209933838; C7), the free-state of Saxony and Helmholtz Munich.

Competing interests: Shahaf Peleg is a co-founder of Luminova Biotech. This does not alter our adherence to PLOS ONE policies on sharing data and materials.

deregulation, neurodegeneration, muscle function and related metabolism, heart diastolic dysfunction and others in mice [11–13]. Therefore, a strong link between inhibiting histone deacetylases (HDACs), increased histone acetylation and disease therapy was suggested.

Nonetheless, there is growing evidence in recent years that many non-histone proteins are acetylated as well [9, 14–17]. These proteins are involved in various cellular pathways. Of note, HDACs were shown to be able to deacetylate many of these non-histone proteins and thus were more accurately termed lysine deacetylases (KDACs) [16]. As such, it is possible that KDAC inhibitors (KDACi) could impact a myriad of non-epigenetic pathways.

Previously, we have shown that sodium butyrate (SB) induces rapid and transient oxygen consumption increase in the heads of *Drosophila melanogaster* while other work showed similar induction in colon-derived cell lines [18]. The rapid increase was detected already after several minutes, suggesting that it may be too rapid to be dependent on new gene transcription following protein translation that is mediated by histone acetylation changes [19]. Interestingly, previous studies have shown that butyrate can induce increased non-histone protein acetylation [17]. As many of these acetylated proteins are known to be metabolic enzymes, we hypothesized that butyrate may cause an increase in the acetylation levels of metabolic proteins, which may underlie the observed rapid increase in oxygen consumption rate (OCR). We expected that butyrate will impact the levels of metabolites associated with mitochondrial oxygen consumption.

Results

Oxygen consumption assessment in fly heads

We have previously measured the impact of SB on OCR in a Seahorse X24 analyzer [20–22]. In the present study, we first re-assessed the kinetics of SB-induced OCR increased using the new Seahorse XFe24 analyzer with improved sensor capacity. Furthermore, we improved the pH adjustment of media containing SB/vehicle (see methods). We also tested lower and higher concentrations of SB (3mM, 30mM). Using the improved protocol, we observed that compared to previously published data, 15mM SB induced an even more rapid OCR increase, peaking as early as 22.5 minutes (4^{th} measurement compared with 6^{th} measurement in Becker et al. [20]) (Fig 1 and S1B Fig in S1 File). Additionally, 30mM SB induced a stronger and prolonged OCR increase (Fig 1 and S1C Fig in S1 File), whereas, 3mM SB treatment was insufficient and did not result in an OCR increase (Fig 1 and S1A Fig in S1 File). Similarly, under the improved protocol, vehicle group showed relatively more stable OCR levels throughout the experiment (Fig 1), compared to our previous work where the vehicle measurements displayed a mild and transient increase in OCR. It is noteworthy that the addition of the SB slightly cause a reduction of the pH of the media, while the pH of the buffer of 3mM and 15Mm were similar (S2 Fig in S1 File). Collectively, the improved protocol supported the notion of earlier impact of SB on OCR alongside an improved control group.

Proteome and acetylome measurements in fly heads

We next assessed the impact of SB treatment on the fly head proteome and acetylome while focusing on potential alterations during 20 minutes of 15mM SB treatment.

It was hypothesized, that SB, as a KDACi, alters non-histone protein acetylation in fly heads, which leads to increased oxygen consumption, and that the observed phenotype is not caused by any transcriptional changes due to the short treatment window of only 20 minutes [19]. As expected, our proteome comparison between vehicle and 15mM SB of 2827 detectable proteins shows no significant abundance change in flies' heads after 20 minutes of incubation with SB (Fig 2A). Specifically, we detected no significant changes key metabolic enzymes in the TCA cycle metabolism and in the respiratory complexes I-IV (Fig 2C–2K and 2L–2P).

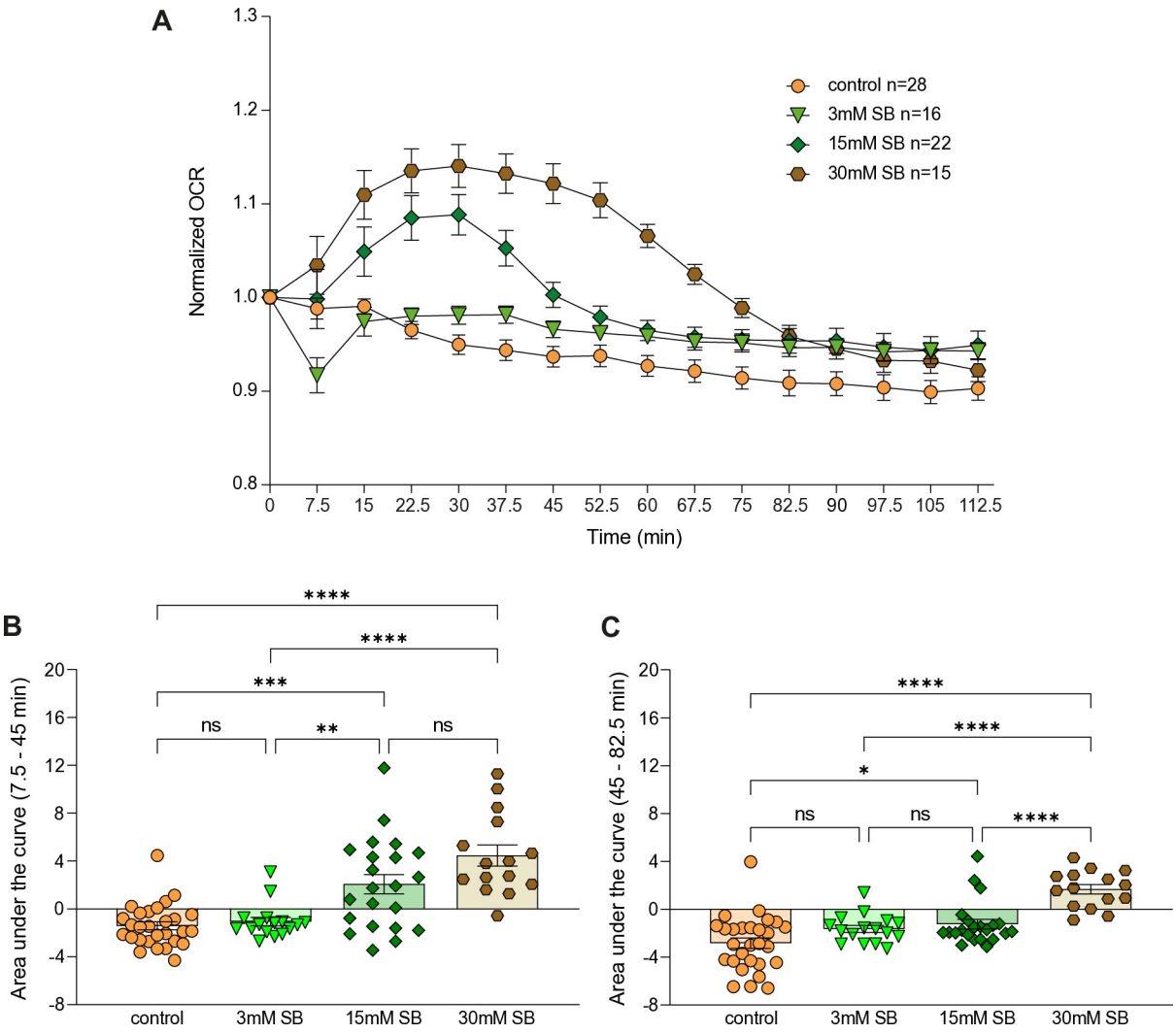

Fig 1. Sodium butyrate rapidly increase oxygen consumption in a dosage dependent manner. (A) Quantification of oxygen consumption levels upon addition of SB. Time zero refers to the last measure prior to the addition of vehicle/SB. (B+C) Area under the curve for each condition plotted in a scatter plot for the 2–7 (7.5–45 minutes) measurements (B) after the injection and 7–12 (45–82.5 minutes) measurements (C) after the injection. Control (orange, n = 28), 3mM SB (light green, n = 16), 15mM SB (dark green, n = 22), 30mM SB (brown, n = 15). Error bars indicate standard error of mean in all graphs. One-way ANOVA, Tukey´s post-hoc test, ns $p>0.05$; * $p\leq0.05$; ** $p\leq0.01$; *** $p\leq0.001$; **** $p\leq0.0001$. Detailed statistical information is presented in S1 and S2 Tables in S1 File. Each measurement was normalized to the first measurement (time point '0'), which is the measurement prior to the introduction of the vehicle/SB/.

https://doi.org/10.1371/journal.pone.0315892.g001

Nonetheless, SB has been previously shown to be a KDAC inhibitor that affects protein acetylation, which is more rapid and dynamic compared with overall protein abundance alterations [23–26]. Dynamic protein acetylation itself has been shown to impact metabolic regulation [27–29]. Therefore, we next measured the protein acetylome after SB/vehicle treatment at 20 min. interestingly, no significant alterations were found among 267 different proteins harboring 557 acetylation sites (Fig 2B). Collectively, we found no impact of SB neither on protein levels nor on protein acetylation at the peak of OCR increase in flies' heads.

As butyrate does not impact protein abundance and protein acetylation, at least at the 20 min mark, we wondered if the heads can utilize butyrate as a metabolite. Previous work showed that SB is used as a metabolite in colonocytes and influences mitochondrial function,

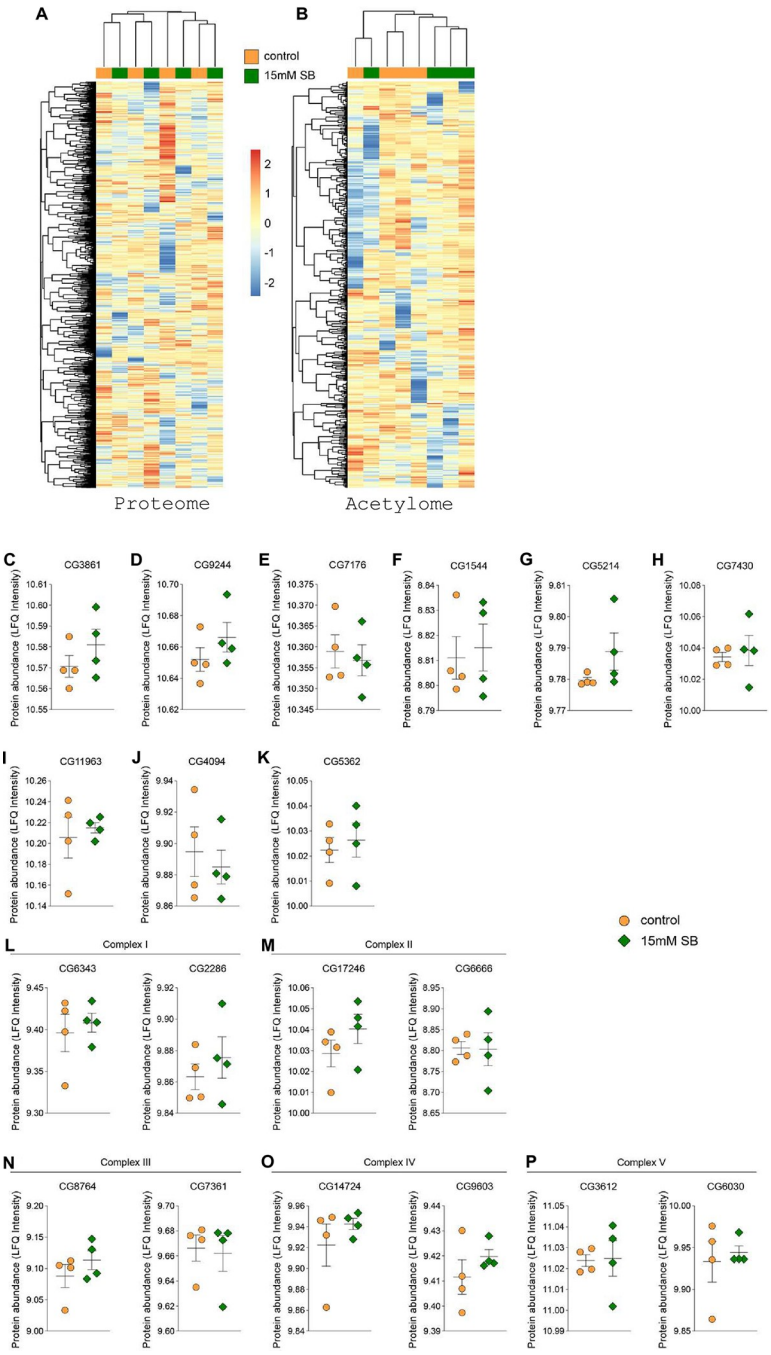

Fig 2. Sodium butyrate does not impact the levels of proteins and acetylation of proteins after 20 minutes. (A) Heatmap showing comparison of 2827 detected proteins between control (orange, n = 4) and 15mM SB (green, n = 4) treated fly heads after 20 min. (B) Heatmap comparing 557 detected acetylation sites of 267 proteins between control (orange, n = 4) and 15mM SB (green, n = 4) treated fly heads after 20 min. FC (fold change). Levels of key mitochondrial proteins related to TCA cycle were not significantly altered after 20 min between control (orange, n = 4) and 15mM SB (green, n = 4) group. Genes encoding proteins are as follows: (C) CG3861 (Citrate synthase), (D) CG9244 (Aconitate hydratase), (E) CG7176 (Isocitrate dehydrogenase), (F) CG1544 (2-oxoglutarate dehydrogenase), (G) CG5214 (Dihydrolipoyllysine-residue succinyltransferase), (H) CG7430 (Dihydrolipoyl dehydrogenase), (I) CG11963 (Succinyl-CoA ligase), (J) CG4094 (Fumarate hydratase), (K) CG5362 (Malate dehydrogenase). Error bars indicate ±S.E.M in all graphs. Student's t-test was performed and detailed statistical information is presented in S3 Table in S1 File. Levels of key mitochondrial proteins were not significantly altered after 20 min between control (orange, n = 4) and 15mM SB (green, n = 4) group. Genes encoding proteins are as follows: (L) Complex I: CG6343 (ND-42), CG2286 (ND-75), (M) Complex II: CG17246 (SdhA), CG6666 (SdhC), (N) Complex III: CG8764 (Ox),

CG7361 (Rieske), (O) Complex IV: CG14724 (COX5A), CG9603 (COX7A) and (P) Complex V. Error bars indicate ±S.E.M in all graphs. Student's t-test was performed and detailed statistical information is presented in S3 Table in S1 File.

https://doi.org/10.1371/journal.pone.0315892.g002

e.g., in the liver [23, 26]. As such, we hypothesized that butyrate could be utilized as an energy source in the fly heads.

The addition of pyruvate and proline transiently increase OCR

We next tested metabolites that are known to affect the electron transport chain and hence the OCR. In a similar experimental design described for the SB treatment, we added pyruvate and proline as positive control to fly heads. Indeed, treatment of fly heads with pyruvate and proline, two metabolites that are known substrates for the mitochondria of flies, revealed kinetics similar to the responses observed after SB treatment (Fig 3). The similarity of the kinetic of pyruvate/proline and SB suggests that SB might be used as mitochondrial substrate in the fly heads.

Assessment of the fly metabolome following treatment with $^{13}C_4$-labeled sodium butyrate

To test this hypothesis, we incubated fly heads in a buffer containing $^{13}C_4$-labeled 15mM SB and the assessed incorporation of labeled carbon atoms into metabolites by using liquid chromatography-mass spectrometry (LC-MS) at three distinct time points (0 min, 20 min, and 60 min). Of note, fly heads were continuously exposed to $^{13}C_4$-labeled 15mM SB for the entire duration of each experiment. As expected, we found substantial increase in the pool sizes of butyric acid, butyryl coenzyme A (CoA), and 3-hydroxybutyryl-CoA (Fig 4B–4D) showing nearly 100% incorporation of heavy labeled carbons (S3 and S4A-S4C Figs in S1 File). Additionally, we observed increased $^{13}C_2$ labeling of acetyl-CoA over time (Fig 5A and S4D Fig in S1 File). In line with these results, we also observed a substantial increase in stable isotope labeling in all detected TCA metabolites (Fig 5B–5H and S4E-S4M Fig in S1 File), indicating that the carbons from the butyrate have been rapidly incorporated into the TCA cycle specifically via β-oxidation to acetyl-CoA. Notably, the overall incorporation of $^{13}C_4$ continued to increase from 20 to 60 min (Fig 5). Lastly, we did not observe ^{13}C incorporation in this time frame into other metabolites such as the amino acids arginine, aspartate, glutamate and proline (S5 Fig in S1 File).

Discussion

In this work, we tested the impact of SB on molecular metabolism processes that might explain the rapid increase in whole fly head OCR. Firstly, we used an improved method to measure OCR in response to SB treatment. The new Seahorse analyzer, manual OCR calculation (see methods) and improved pH control have led to a more stable result for vehicle group measurements, compared with previously published data [20]. Furthermore, the improved method revealed an earlier increase of OCR in response to SB treatment, namely already after 3–4 measurements (22.5–30 minutes), which supported the notion that the OCR increase is independent of histone-mediated transcription and following translation [17, 22]. Additionally, we showed that the increased OCR is SB is dose-dependent. For example, using higher 30mM SB concentration results in stronger and prolonged OCR increase in fly heads. We suggest that molecular studies could benefit from using increased dosage of SB that may assist uncovering the impacted molecular pathways, as the magnitude of response is elevated.

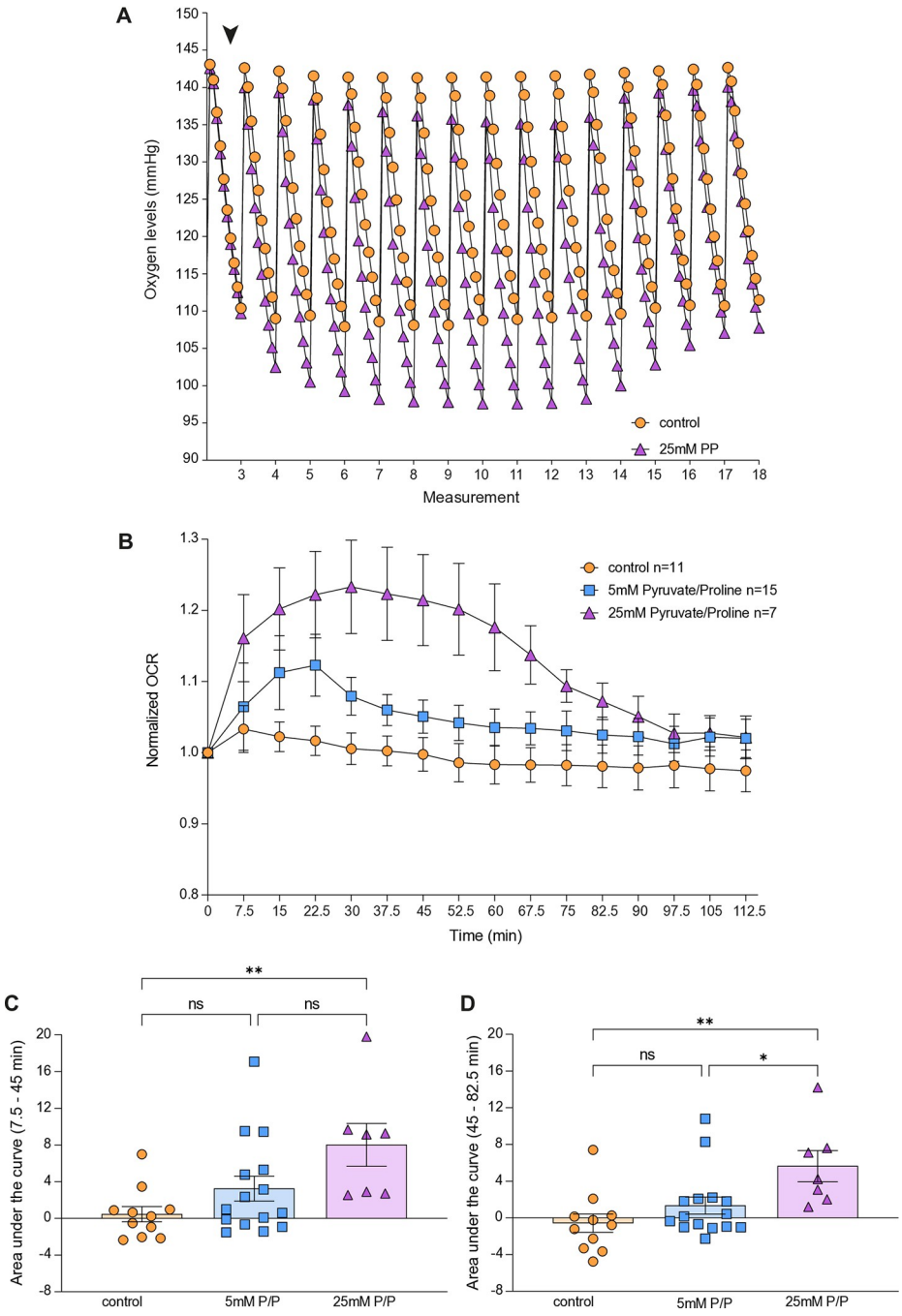

Fig 3. Pyruvate and proline rapidly and transiently increase oxygen consumption in fly heads. (A) Representative tracing for oxygen level changes in control and 25mM pyruvate and proline (PP)-treated fly heads. Each measurement lasted 2 min and consisted of 10 sub-measurements (ticks). The last measurement before (3) and the measurements after injection (4–18) are shown. The arrowhead indicates the addition of PP or control. (B) Quantification of OCR based on (A). (C+D) Area under the curve for each condition plotted in a scatter plot for the (C) 2–7 (7.5–45 minutes) measurements or (D) 7–12 (45–82.5 minutes) measurements after the injection. Control (orange, n = 11), 5mM PP (blue, n = 15), 25mM PP (purple, n = 7). One-way ANOVA, Tukey´s post hoc test, ns $p>0.05$; * $p\leq0.05$; ** $p\leq0.01$. Error bars indicate ±S.E.M in all graphs. Detailed statistical information is presented in S4 and S5 Tables in S1 File. Each measurement was normalized to the first measurement (time point '0'), which is the measurement prior to the introduction of the vehicle/pyruvate+proline.

https://doi.org/10.1371/journal.pone.0315892.g003

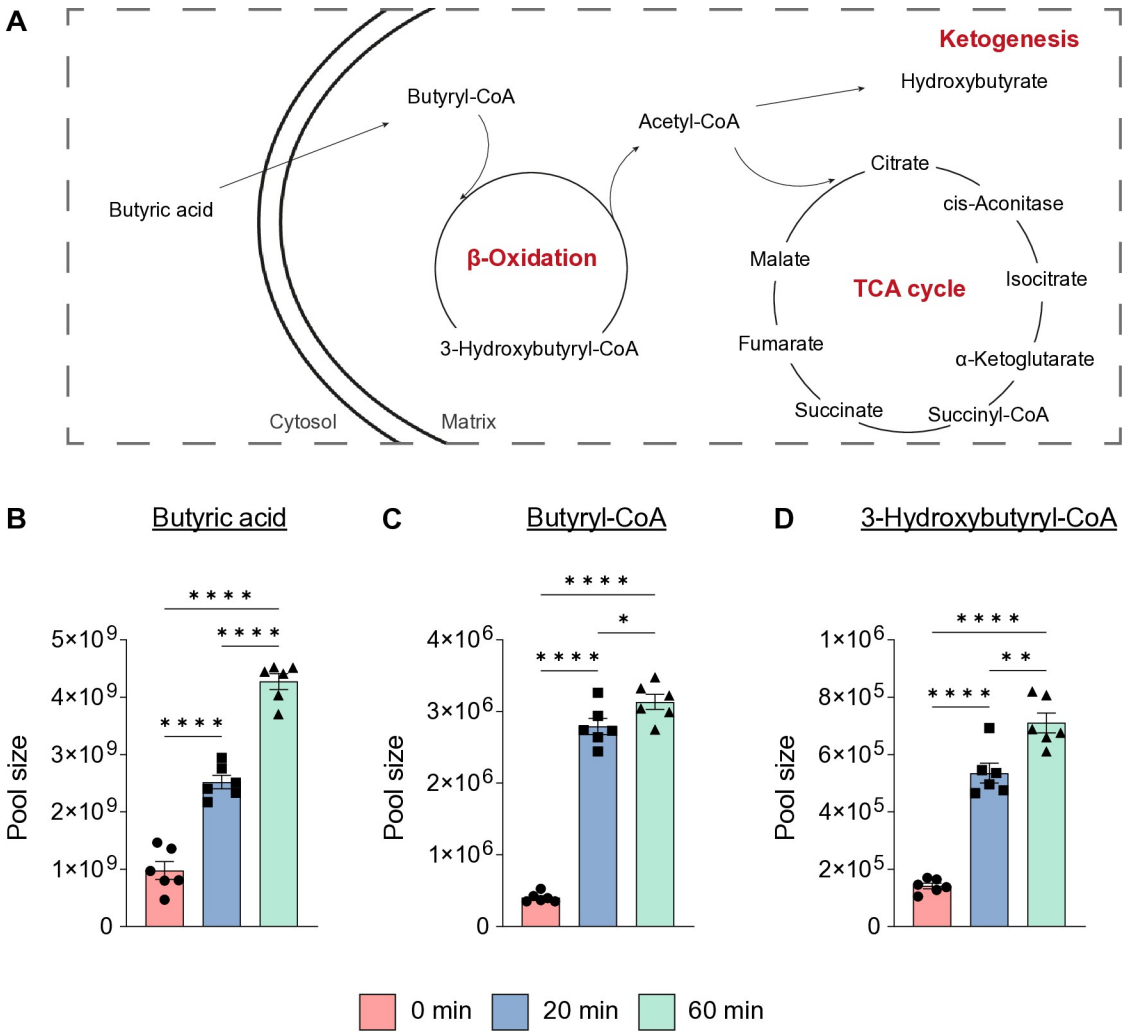

Fig 4. Butyrate is rapidly incorporated into butyric derivatives. (A) Schematic overview of key metabolic pathways (red) involving the measured metabolites. (B-D) Changes in pool size in response to $^{13}C_4$-labeled SB treatment in fly heads over time (red, 0 min; blue, 20 min; green, 60 min). n = 6 for all metabolites. Error bars indicate ±S.E.M in all graphs. One-way ANOVA, Tukey´s post-hoc test, ns $p>0.05$; * $p\leq0.05$; ** $p \leq 0.01$; *** $p\leq0.001$; **** $p\leq0.0001$. Detailed statistical information is presented in S6 Table in S1 File.

https://doi.org/10.1371/journal.pone.0315892.g004

Notably, we observed that similarly to SB, pyruvate and proline induce similar increased OCR kinetics. Interestingly, both responses are transient and are back to normal OCR levels after over one hour. The reason for this is not clear and should be further investigated. It is evident that, at least with SB, sufficient SB is still present in the buffer after 60 minutes (S6 Fig in S1 File). However, it is possible that feedback loops aimed to control mitochondrial respiration are active to counter SB's impact on the OCR. More work is needed to understand the mechanism that reset the OCR levels back to their basal state.

In line with our initial hypothesis, we found no changes in protein abundance after 20 minutes of SB treatment. This is supported by the fact that such time frame is likely too short for the transcription and translation of proteins to increase the OCR [19]. However surprisingly, in contrast to our initial hypothesis, we also observed no significant alterations in protein acetylation in this time frame. Protein acetylation was shown to modulate metabolic activity, and acetylation itself is rapid and dynamic [17, 28, 29]. While it is possible that a broader mass

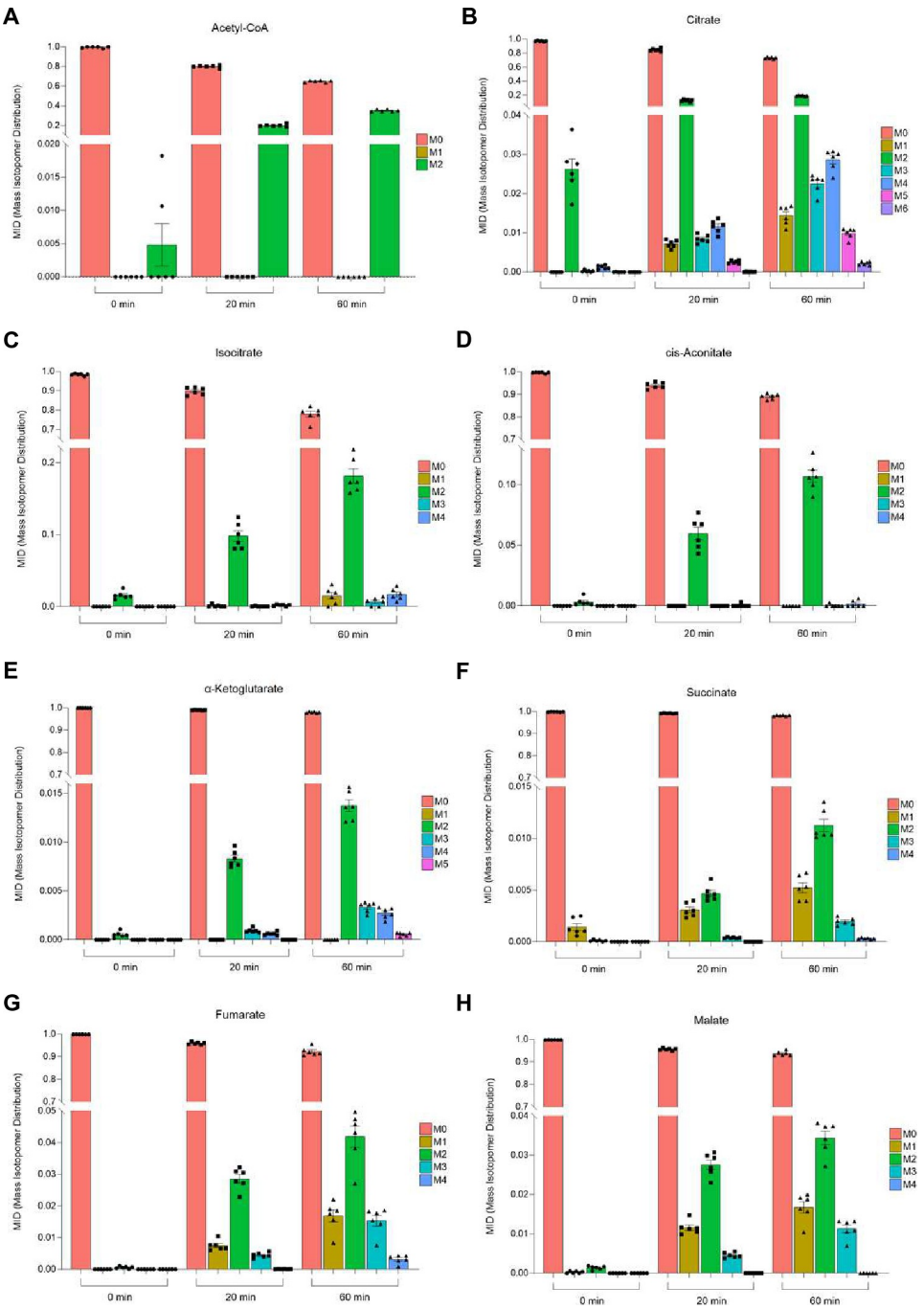

Fig 5. Butyrate is rapidly incorporated into TCA cycle metabolites. (A) Analysis of Mass Isotopomer Distribution (MID) of acetyl-CoA. $^{13}C_4$-sodium butyrate treatment to determine its incorporation at different time points by mass spectrometry. (B-H) Analysis of Mass Isotopomer Distribution (MID) in TCA cycle metabolites after $^{13}C_4$-SB treatment to determine its incorporation over time by mass spectrometry. n = 6 for all metabolites and time points. M0 unlabeled mass of isotope, M+n native metabolite mass + number of isotopically labeled carbons. Error bars indicate ±S.E.M in all graphs. Detailed statistical analysis was performed using one-way ANOVA, Tukey´s post-hoc test, results are presented in S7 Table in S1 File.

https://doi.org/10.1371/journal.pone.0315892.g005

spectrometric coverage would reveal protein acetylation changes, our data support the notion that SB, at least within the measured time frame, does not induce increased acetylation that may be linked with the increased OCR. This is important as previous studies tested short-term impact of SB in the brain, for example on memory formation enhancement, and linked it with acetylation increase [11]. However, our data suggest that SB may in fact act as a metabolic boost and that such a boost may be the underlying benefit for previously described therapeutic attributes of SB.

Our results further support the idea that butyrate is rapidly incorporated specifically into β-oxidation and TCA cycle metabolites. We observed a clear ^{13}C incorporation in the TCA cycle metabolites. Notably, the measurement intensity for succinyl-CoA was low, while oxaloacetate was not detected at all, which might indicate lower stability of these metabolites, therefore making it more difficult to detect ^{13}C. Nonetheless, our data clearly shows a specific and gradual accumulation of ^{13}C in acetyl-CoA and TCA metabolites. In fact, already at so-called time point 0, we observed ^{13}C incorporation. This might be attributed to the fact that even the short exposure to ^{13}C labeled butyrate, while collecting the samples, is sufficient to cause ^{13}C incorporation into the TCA metabolites. Overall, this data shows a correlation between fueling the oxidation and TCA cycle in a similar time frame to increased OCR in fly heads.

The enrichments for most metabolites in the TCA cycle following citric acid are rather low. Accordingly, we would postulate that the mitochondrially incorporated $^{13}C_2$ of each unit from the beta-oxidized $^{13}C_4$ butyrate molecule, end up, after being converted to $^{13}C_2$ acetyl-CoA, in the TCA cycle where it reaches the first product, namely citrate. As can be further seen, the enrichment does not seem to be forwarded linearly into the following TCA cycle intermediates, since the enrichment rate of cis-aconitate, isocitrate and even more α -ketoglutarate and followers, are by far lower than the 20% M2 enrichment observed for citrate (e.g., 1.5% M2 for α-ketoglutarate, Fig 5E). One assumption that can be drawn from these disproportional enrichments observed would be, that the synthetized citrate may be immediately exported to the cytosol where it might be degraded and converted through the ATP citrate lyase (ACLY) into oxaloacetate and $^{13}C_2$ acetyl-CoA. While the oxaloacetate carbon can be reimported to the mitochondrion via malate and pyruvate, the obtained $^{13}C_2$ acetyl-CoA might be converted into newly synthetized fatty acids. Unfortunately, we cannot proof this assumption, since we did not measure fatty acids and hence cannot determine their increased ^{13}C-enrichment levels in this study.

Butyrate has been previously suggested as a drug for treating diseases such as neurodegenerative maladies and sarcopenia. It is possible that some of the benefits of butyrate that were previously described may be attributed to direct metabolic boost. Although not tested here, butyrate can increase the levels of key metabolites such as ATP which may be lower in such maladies. Furthermore, the incorporation of butyrate in key TCA metabolites might benefit health span as for example in mice, the addition of α-ketoglutarate promotes healthy lifespan associated with reduced inflammation.

In summary, we show that SB rapidly incorporates into central metabolic pathways in fly heads while, at least within the studied time frame, causing no visible impact on protein acetylation. Our data supports the notion that the role of SB as a therapy mainly via inhibiting KDAC to cause increased protein acetylation should be revisited. Instead, we rationalize that SB may act, at least acutely, as a transient metabolic boost and thus lead to improved memory performance as previously described. Nonetheless, more causal evidence is needed to tightly link the observed OCR increase induction by SB and rapid metabolic alterations in the context of whole tissue.

Methods

Fly strains

The *Drosophila melanogaster* strain w^{1118} was maintained and cultivated at 25˚C with 60% humidity and a 12 h light/ 12 h dark cycle on normal fly food (11 l H2O, 97.5 g Agar, 975 g corn flour, 112.5 g soy flour, 225 g yeast, 975 g melasse, 487.5 g malt, 311.25 ml Nipagin, 221.25 ml acid mix) and transferred to new vials with fresh fly food at different time periods. In order to select flies according to gender, flies were briefly sedated with CO_2. Male flies were selected for the study at the age of 7–9 days.

Oxygen consumption measurements

Oxygen consumption measurements were done using Seahorse XFe24 Analyzer and the corresponding XFe24 island plates as previously described [22] with the following modifications:

Solutions were freshly prepared on experimental day and pH was adjusted to 7.15 (buffer) and 6.95 (SB) with NaOH or HCl at experimental temperature of 31˚C. The plate wells and the injection ports were inspected for air bubbles, which were removed using a pipette if necessary.

The automatic FIXED algorithm, which was used for the XF24 machine [21], is absent in the new XFe24 machine and therefore OCR was analyzed by calculating the decrease in oxygen level by dividing tick 5 by tick 2 and normalized to the last basal measurement before injection (third total measurement).

Each measurement was normalized to the first measurement (time point '0'), which is the measurement prior to the introduction of the vehicle/SB/pyruvate+proline.

Plate preparation for omics

Plate preparation for proteome/acetylome analyses was done as described for the Seahorse XFe24 Analyzer, with the following additions [21]. The plate was incubated at 31˚C for 20 min to reflect the three basal measurements during the OCR experiments. Afterwards, vehicle or SB solution was carefully added to fly heads and an incubation step at 31˚C of 20 min or 60 min followed. Subsequently, plates were removed from the incubator and supernatant was discarded. The wells were washed with water and immediately frozen by using liquid nitrogen. Fly heads were removed on dry ice from plates by using forceps and stored in reaction tubes at– 80˚C until further analysis. 16 fly heads corresponded to one biological sample (n) for metabolome analysis, whereas 1000 fly heads were needed for proteome and acetylome analysis.

Proteome and acetylome analysis

High-resolution mass spectrometry was used to identify potential lysine acetylation sites on proteins and acetylation changes in fly heads as previously described [22].

Briefly, 100 mg of frozen fly heads were homogenized in 300 μl lysis buffer as previously described [22]. To reduce disulfide bonds, samples were treated with the reducing agent dithiothreitol (DTT), followed by a treatment with iodoacetamide (IAA) to alkylate free cysteines.

Samples were digested for 5 h with Lys-C and with trypsin. The eluted peptide concentration was measured by NanoDrop One^{C} spectrophotometer and equal concentration of peptides were incubated with 45 μl anti-acetyllysine antibody (ICP0388, Immunechem) overnight at 4˚C. Beads were washed four times with phosphate-buffered saline (PBS)/Tween 0.1% and then four times with PBS. Acetylated peptides were eluted from beads with 125 μl 0.1%

Trifluoroacetic acid (TFA). For proteome analysis 20 μl of each sample were taken before enrichment for acetylated lysines and were diluted with 80 μl 0.1% TFA.

LC-MS/MS measurements were performed as described previously [30]. Briefly, for full proteome measurement, 0.25 μg purified peptides were injected into an Ultimate 3000 RSLCnano system coupled to a Q-Exactive HF-X mass spectrometer (Thermo Fisher Scientific), while for acetylome measurements the complete peptide sample derived after acetylome enrichment (concentration unknown) was injected. The Q-Exactive HF-X mass spectrometer was operated in the data-dependent acquisition and positive ionization mode using a 120 minute linear LC gradient. Peptide identification and quantification were performed using MaxQuant (version 1.6.3.4). MS2 spectra were searched against the Uniprot *Drosophila melanogaster* proteome database (UP000000803, 21923 entries, download at 22.3.2019). For full proteome analyses, carbamidomethylated cysteine was set as fixed modification and oxidation of methionine and N-terminal protein acetylation as variable modifications. For the acetylome data, additionally Lysine acetylation was set as variable modifications.

Protein abundances were calculated using the label-free quantification algorithm from MaxQuant [31]. The intensities of lysine-acetylated peptides from the "modificationSpecificPeptides.txt" table were used to quantify the relative abundances of acetylation site. Student's t-test was used to identify the differentially expressed proteins and lysine-acetylated peptides between control and SB. The resulting p values were adjusted by the Benjamini–Hochberg algorithm the FDR [32]. For heatmap generation, the intensity matrix was scaled row-wise. Correlation distance and Euclidean distance were used to generate dendrograms on rows and columns respectively. The statistical analyses were performed using R 4.1.0 (R Core Team, 2021).

Metabolome analysis

Heavy-labeled sodium butyrate-$^{13}C_4$ was used for all metabolome-experiments. Semi-targeted liquid chromatography-high-resolution mass spectrometry (LC-HRMS) analysis of short chain fatty acyl coenzyme A species (Acyl-CoAs) was applied. The LC-HRMS analysis of Acyl-CoAs was performed using an adapted protocol [33].

In brief, the dried metabolite extract was re-suspended in 50 μl of LC-MS-grade water (Optima-Grade, Thermo Fisher Scientific). After 15 min incubation on a thermomixer at 4˚C and a 5 min centrifugation at 16,000 x g at 4˚C, the cleared supernatants were transferred to glass autosampler vials with 300 μl glass inserts (Chromatography Accessories Trott, Germany).

For the LC-HRMS analysis, 1 μl of the sample was injected onto a 30 x 2.1 mm BEH Amide UPLC column (Waters) with 1.7 μm particle size. The gradient elution ran in a quaternary Vanquish Flex LC system (Thermo Fisher Scientific) with a flow rate of 500 μl/min using a quaternary buffer system consisting of buffer A 5 mM ammonium acetate (Sigma) in LC-MS-grade water (Optima-Grade, Thermo Fisher Scientific); buffer B consisted of 5 mM ammonium acetate (Sigma) in 95% acetonitrile (Optima-grade, Thermo Fisher Scientific); buffer C consisted of 0.1% phosphoric acid (85%, VWR) in 60% acetonitrile (acidic wash) and buffer D of 50% acetonitrile (neutral wash). The column temperature was set to 30˚C, while the LC gradient was: 85% B for 1 min, 85–70% B 1–3 min; 70–50% B 3–3.2 min; holding 50% B till 5 min; 100% C 5.1–8 min, 100% D 8.1–10 min; followed by re-equilibration with 15% A and 85% B 10.1–13 min. The mass spectrometer (Q-Exactive HF, Thermo Fisher Scientific) was operating in positive ionization mode recording the mass range m/z 760–1800. The heated electrospray ionization (ESI) source settings of the mass spectrometer were set to: Spray voltage 3.5 kV, capillary temperature 300˚C, sheath gas flow 50 AU, aux gas flow 15 AU at a temperature of 350˚C and the sweep gas to 3 AU. The RF-lens was set to a value of 55.

The identity of acetyl-CoA and malonyl-CoA was validated by authentic ^{13}C labeled reference compounds, which were run before. Other Acyl-CoAs annotations were validated by using *E. coli* reference material matching exact mass and reporter ions from PRM experiments. Peak areas of $[M + H]^+$ ions and corresponding isotopomeres were extracted using a mass accuracy (<5 ppm) and a retention time tolerance of <0.05 min.

Semi-targeted LC-HRMS analysis of amine-containing metabolites

The LC-HRMS analysis of amine-containing compounds was performed using an adapted benzoylchlorid-based derivatization method [34].

In brief: The polar fraction of the metabolite extract was re-suspended in 200 μl of LC-MS-grade water (Optima-Grade, Thermo Fisher Scientific) and incubated at 4˚C for 15 min on a thermomixer. The re-suspended extract was centrifuged for 5 min at 16,000 x g at 4˚C and 50 μl of the cleared supernatant was mixed with 25 μl of 100 mM sodium carbonate (Sigma), followed by the addition of 25 μl 2% [v/v] benzoylchloride (Sigma) in acetonitrile (Optima-Grade, Thermo Fisher Scientific). Samples were vortexed and kept at 20˚C until analysis. After a 5 min centrifugation at 16,000 x g at 20˚C, the cleared supernatant was transferred to glass autosampler vials with 300 μl glass inserts (Chromatography Accessories Trott, Germany).

For the LC-HRMS analysis, 1 μl of the derivatized sample was injected onto a 100 x 2.1 mm HSS T3 UPLC column (Waters) with 1.8 μm particle size. The gradient elution ran in a binary Vanquish Horizon LC system (Thermo Fisher Scientific) with a flow rate of 400 μl/min using a binary buffer system consisting of buffer A:10 mM ammonium formate (Sigma), 0.15% [v/v] formic acid (Sigma) in LC-MS-grade water (Optima-Grade, Thermo Fisher Scientific) and buffer B consisted solely of acetonitrile (Optima-grade, Thermo Fisher-Scientific). The column temperature was set to 40˚C, while the LC gradient was: 0% B at 0 min, 0–15% B 0–4.1 min; 15–17% B 4.1–4.5 min; 17–55% B 4.5–11 min; 55–70% B 11–11.5 min, 70–100% B 11.5–13 min; B 100% 13–14 min; 100–0% B 14–14.1 min; 0% B 14.1–19 min; 0% B. The mass spectrometer (Q-Exactive Plus, Thermo Fisher Scientific) was operating in positive ionization mode recording the mass range m/z 100–1000. The heated ESI source settings of the mass spectrometer were set to: Spray voltage 3.5 kV, capillary temperature 300˚C, sheath gas flow 60 AU, aux gas flow 20 AU at a temperature of 330˚C and the sweep gas to 2 AU. The RF-lens was set to a value of 60.

The identity of each compound was validated by authentic reference compounds, which were run before and after every sequence. Peak areas of [M + nBz + H]+ ions and isotopomers were extracted using a mass accuracy (<5 ppm) and a retention time tolerance of <0.05 min.

Anion-Exchange Chromatography Mass Spectrometry (AEX-MS) for the analysis of anionic metabolites

Extracted metabolites were re-suspended in 200 μl of Optima UPLC/MS grade water (Thermo Fisher Scientific). After 15 min incubation on a thermomixer at 4˚C and a 5 min centrifugation at 16,000 x g at 4˚C, 100 μl of the cleared supernatant were transferred to polypropylene autosampler vials (Chromatography Accessories Trott).

The samples were analyzed using a Dionex ion chromatography system (Integrion, Thermo Fisher Scientific) as described previously [35]. In brief, 5 μl of polar metabolite extract was injected in full loop mode using an overfill factor of 1, onto a Dionex IonPac AS11-HC column (2 mm × 250 mm, 4 μm particle size, Thermo Fisher Scientific) equipped with a Dionex IonPac AG11-HC guard column (2 mm × 50 mm, 4 μm, Thermo Fisher Scientific). The column temperature was held at 30˚C, while the auto sampler was set to 6˚C. A potassium hydroxide gradient was generated using a potassium hydroxide cartridge (Eluent Generator, Thermo

Scientific), which was supplied with deionized water. The metabolite separation was carried at a flow rate of 380 μl/min, applying the following gradient conditions: 0–3 min, 10 mM KOH; 3–12 min, 10–50 mM KOH; 12–19 min, 50–100 mM KOH, 19–21 min, 100 mM KOH, 21–22 min, 100–10 mM KOH. The column was re-equilibrated at 10 mM for 8 min.

For the analysis of metabolic pool sizes the eluting compounds were detected in negative ion mode using full scan measurements in the mass range m/z 50–750 on a Q-Exactive HF high resolution MS (Thermo Fisher Scientific). The heated ESI source settings of the mass spectrometer were: Spray voltage 3.2 kV, capillary temperature was set to 275˚C, sheath gas flow 70 AU, aux gas flow 15 AU at a temperature of 350˚C and a sweep gas flow of 0 AU. The S-lens was set to a value of 50.

The identity of each compound was validated by authentic reference compounds, which were measured at the beginning and the end of the sequence.

The LC/IC-MS data analysis was performed using the open source software El Maven 0.12.0 [36]. For this purpose, Thermo raw mass spectra files were converted to mzML format using MSConvert 3.0.22060 [37] (Proteowizard). Molecular ion and the corresponding isotopologue mass peaks of every required compound were extracted and integrated using the underlying algorithm within El Maven, only in rare cases isotopologue mass peaks were manually re-integrated. Extracted ion chromatograms were generated with a mass accuracy of <5 ppm and a retention time (RT) tolerance of <0.05 min as compared to the independently measured reference compounds. Afterwards, Isotopomer distribution was corrected for natural abundant isotopes with the IsoCorrectoR [38] package in R. If no independent 12C experiments were carried out, where the pool size is determined from the obtained peak area of the 12C monoisotopologue, the pool size determination was carried out by summing up the peak areas of all detectable isotopologues per compound. These areas were then normalized, as performed for un-traced 12C experiments, to the internal standards, which were added to the extraction buffer, followed by a normalization to the protein content or the cell number of the analyzed samples. The relative isotope distribution of each isotopologue was calculated from the proportion of the peak area of each isotopologue towards the sum of all detectable isotopologues. The 13C enrichment, namely the area attributed to 13C molecules traced in the detected isotopologues, was calculated by multiplying the peak area of each isotopologue with the proportion of the 13C and the 12C carbon number for the corresponding isotopologue (the 12C and 13C monoisotopologue areas were multiplied with 0 and 1 respectively). The obtained 13C area of each isotopologue are summed up, providing the peak area fraction associated to 13C atoms in the compound. Dividing this absolute 13C area by the summed area of all isotopologues provides the relative 13C enrichment factor.

Supporting information

S1 File.
(DOCX)

Acknowledgments

We would like to thank our technicians Verena Hofer-Pretz and Paula Becker for performing many of the experiments for this study, as well as for managing the laboratory conditions that enabled this work. Further, the authors thank Franziska Hackbarth and Nina Lomp for technical assistance at the BayBioMS and acknowledge Miriam Abele for support in mass spectrometeric data acquisiton.

Author Contributions

Conceptualization: Shahaf Peleg.

Data curation: Annika Müller-Eigner, Benedikt Gille, Frederik Dethloff, Chen Meng, Christina Ludwig, Patrick Giavalisco.

Formal analysis: Annika Müller-Eigner, Frederik Dethloff, Chen Meng, Christina Ludwig.

Funding acquisition: Shahaf Peleg.

Investigation: Annika Müller-Eigner, Frederik Dethloff, Chen Meng, Christina Ludwig.

Methodology: Annika Müller-Eigner, Benedikt Gille, Frederik Dethloff, Chen Meng.

Resources: John T. Heiker, Patrick Giavalisco, Shahaf Peleg.

Software: John T. Heiker, Patrick Giavalisco.

Supervision: Christina Ludwig, John T. Heiker, Patrick Giavalisco, Shahaf Peleg.

Validation: Annika Müller-Eigner, Frederik Dethloff, Shahaf Peleg.

Visualization: Annika Müller-Eigner, Chen Meng.

Writing – original draft: Annika Müller-Eigner, Shahaf Peleg.

Writing – review & editing: Annika Müller-Eigner, Benedikt Gille, Frederik Dethloff, Chen Meng, Christina Ludwig, John T. Heiker, Patrick Giavalisco, Shahaf Peleg.

References

1. Kornberg RD. Chromatin structure: a repeating unit of histones and DNA. Science 1974; 184 (4139):868–71. https://doi.org/10.1126/science.184.4139.868 PMID: 4825889
2. Kornberg RD, Lorch Y. Twenty-five years of the nucleosome, fundamental particle of the eukaryote chromosome. Cell 1999; 98(3):285–94. https://doi.org/10.1016/s0092-8674(00)81958-3 PMID: 10458604
3. Luger K, Mäder AW, Richmond RK, Sargent DF, Richmond TJ. Crystal structure of the nucleosome core particle at 2.8 A resolution. Nature 1997; 389(6648):251–60. https://doi.org/10.1038/38444 PMID: 9305837
4. Wang K, Liu H, Hu Q, Wang L, Liu J, Zheng Z et al. Epigenetic regulation of aging: implications for interventions of aging and diseases. Signal Transduct Target Ther 2022; 7(1):374. https://doi.org/10.1038/s41392-022-01211-8 PMID: 36336680
5. Strahl BD, Allis CD. The language of covalent histone modifications. Nature 2000; 403(6765):41–5. https://doi.org/10.1038/47412 PMID: 10638745
6. Rice JC, Allis CD. Histone methylation versus histone acetylation: new insights into epigenetic regulation. Curr Opin Cell Biol 2001; 13(3):263–73. https://doi.org/10.1016/s0955-0674(00)00208-8 PMID: 11343896
7. Cedar H, Bergman Y. Linking DNA methylation and histone modification: patterns and paradigms. Nat Rev Genet 2009; 10(5):295–304. https://doi.org/10.1038/nrg2540 PMID: 19308066
8. Berger SL. Gene activation by histone and factor acetyltransferases. Curr Opin Cell Biol 1999; 11 (3):336–41. https://doi.org/10.1016/S0955-0674(99)80046-5 PMID: 10395565
9. Choudhary C, Weinert BT, Nishida Y, Verdin E, Mann M. The growing landscape of lysine acetylation links metabolism and cell signalling. Nat Rev Mol Cell Biol 2014; 15(8):536–50. https://doi.org/10.1038/nrm3841 PMID: 25053359
10. Peleg S, Sananbenesi F, Zovoilis A, Burkhardt S, Bahari-Javan S, Agis-Balboa RC et al. Altered histone acetylation is associated with age-dependent memory impairment in mice. Science 2010; 328 (5979):753–6. https://doi.org/10.1126/science.1186088 PMID: 20448184
11. Fernando WMADB, Martins IJ, Morici M, Bharadwaj P, Rainey-Smith SR, Lim WLF et al. Sodium Butyrate Reduces Brain Amyloid-β Levels and Improves Cognitive Memory Performance in an Alzheimer's Disease Transgenic Mouse Model at an Early Disease Stage. J Alzheimers Dis 2020; 74(1):91–9.

12. Park MJ, Sohrabji F. The histone deacetylase inhibitor, sodium butyrate, exhibits neuroprotective effects for ischemic stroke in middle-aged female rats. J Neuroinflammation 2016; 13(1):300. https://doi.org/10.1186/s12974-016-0765-6 PMID: 27905989

13. Paskova L, Smesny Trtkova K, Fialova B, Benedikova A, Langova K, Kolar Z. Different effect of sodium butyrate on cancer and normal prostate cells. Toxicol In Vitro 2013; 27(5):1489–95. https://doi.org/10.1016/j.tiv.2013.03.002 PMID: 23524101

14. Friedmann DR, Marmorstein R. Structure and mechanism of non-histone protein acetyltransferase enzymes. FEBS J 2013; 280(22):5570–81. https://doi.org/10.1111/febs.12373 PMID: 23742047

15. Drazic A, Myklebust LM, Ree R, Arnesen T. The world of protein acetylation. Biochim Biophys Acta 2016; 1864(10):1372–401. https://doi.org/10.1016/j.bbapap.2016.06.007 PMID: 27296530

16. Imhof A, Peleg S. From HDACi to KDACi: we need to revisit non-epigenetic pathways affected by inhibiting lysine deacetylases in therapy. EMBO Rep 2016; 17(12):1673. https://doi.org/10.15252/embr.201643425 PMID: 27797855

17. Schölz C, Weinert BT, Wagner SA, Beli P, Miyake Y, Qi J et al. Acetylation site specificities of lysine deacetylase inhibitors in human cells. Nat Biotechnol 2015; 33(4):415–23. https://doi.org/10.1038/nbt.3130 PMID: 25751058

18. Bekebrede AF, van Deuren T, Gerrits WJJ, Keijer J, Boer VCJ de. Butyrate Alters Pyruvate Flux and Induces Lipid Accumulation in Cultured Colonocytes. Int J Mol Sci 2021; 22(20). https://doi.org/10.3390/ijms222010937 PMID: 34681598

19. Schwanhäusser B, Busse D, Li N, Dittmar G, Schuchhardt J, Wolf J et al. Global quantification of mammalian gene expression control. Nature 2011; 473(7347):337–42. https://doi.org/10.1038/nature10098 PMID: 21593866

20. Becker L, Nogueira MS, Klima C, Angelis MH de, Peleg S. Rapid and transient oxygen consumption increase following acute HDAC/KDAC inhibition in Drosophila tissue. Sci Rep 2018; 8(1):4199. https://doi.org/10.1038/s41598-018-22674-2 PMID: 29520020

21. Dietz LJ, Venkatasubramani AV, Müller-Eigner A, Hrabe de Angelis M, Imhof A, Becker L et al. Measuring and Interpreting Oxygen Consumption Rates in Whole Fly Head Segments. J Vis Exp 2019; 8(143):4199. https://doi.org/10.3791/58601 PMID: 30663674

22. Peleg S, Feller C, Forne I, Schiller E, Sévin DC, Schauer T et al. Life span extension by targeting a link between metabolism and histone acetylation in Drosophila. EMBO Rep 2016; 17(3):455–69. https://doi.org/10.15252/embr.201541132 PMID: 26781291

23. Donohoe DR, Garge N, Zhang X, Sun W, O'Connell TM, Bunger MK et al. The microbiome and butyrate regulate energy metabolism and autophagy in the mammalian colon. Cell Metab 2011; 13(5):517–26. https://doi.org/10.1016/j.cmet.2011.02.018 PMID: 21531334

24. Li B, Li L, Li M, Lam SM, Wang G, Wu Y et al. Microbiota Depletion Impairs Thermogenesis of Brown Adipose Tissue and Browning of White Adipose Tissue. Cell Rep 2019; 26(10):2720–2737.e5. https://doi.org/10.1016/j.celrep.2019.02.015 PMID: 30840893

25. Li Z, Yi C-X, Katiraei S, Kooijman S, Zhou E, Chung CK et al. Butyrate reduces appetite and activates brown adipose tissue via the gut-brain neural circuit. Gut 2018; 67(7):1269–79. https://doi.org/10.1136/gutjnl-2017-314050 PMID: 29101261

26. Mollica MP, Mattace Raso G, Cavaliere G, Trinchese G, Filippo C de, Aceto S et al. Butyrate Regulates Liver Mitochondrial Function, Efficiency, and Dynamics in Insulin-Resistant Obese Mice. Diabetes 2017; 66(5):1405–18. https://doi.org/10.2337/db16-0924 PMID: 28223285

27. Choudhary C, Kumar C, Gnad F, Nielsen ML, Rehman M, Walther TC et al. Lysine acetylation targets protein complexes and co-regulates major cellular functions. Science 2009; 325(5942):834–40. https://doi.org/10.1126/science.1175371 PMID: 19608861

28. Shang S, Liu J, Hua F. Protein acylation: mechanisms, biological functions and therapeutic targets. Signal Transduct Target Ther 2022; 7(1):396. https://doi.org/10.1038/s41392-022-01245-y PMID: 36577755

29. Zhao S, Xu W, Jiang W, Yu W, Lin Y, Zhang T et al. Regulation of cellular metabolism by protein lysine acetylation. Science 2010; 327(5968):1000–4. https://doi.org/10.1126/science.1179689 PMID: 20167786

30. Müller-Eigner A, Sanz-Moreno A, de-Diego I, Venkatasubramani AV, Langhammer M, Gerlini R et al. Dietary intervention improves health metrics and life expectancy of the genetically obese Titan mouse. Commun Biol 2022; 5(1):408. https://doi.org/10.1038/s42003-022-03339-3 PMID: 35505192

31. Cox J, Hein MY, Luber CA, Paron I, Nagaraj N, Mann M. Accurate proteome-wide label-free quantification by delayed normalization and maximal peptide ratio extraction, termed MaxLFQ. Mol Cell Proteomics 2014; 13(9):2513–26. https://doi.org/10.1074/mcp.M113.031591 PMID: 24942700

32. Benjamini Y, Hochberg Y. Controlling the False Discovery Rate: A Practical and Powerful Approach to Multiple Testing. Journal of the Royal Statistical Society Series B: Statistical Methodology 1995; 57 (1):289–300.

33. Abrankó L, Williamson G, Gardner S, Kerimi A. Comprehensive quantitative analysis of fatty-acyl-Coenzyme A species in biological samples by ultra-high performance liquid chromatography-tandem mass spectrometry harmonizing hydrophilic interaction and reversed phase chromatography. J Chromatogr A 2018; 1534:111–22. https://doi.org/10.1016/j.chroma.2017.12.052 PMID: 29290399

34. Wong J-MT, Malec PA, Mabrouk OS, Ro J, Dus M, Kennedy RT. Benzoyl chloride derivatization with liquid chromatography-mass spectrometry for targeted metabolomics of neurochemicals in biological samples. J Chromatogr A 2016; 1446:78–90. https://doi.org/10.1016/j.chroma.2016.04.006 PMID: 27083258

35. Schwaiger M, Rampler E, Hermann G, Miklos W, Berger W, Koellensperger G. Anion-Exchange Chromatography Coupled to High-Resolution Mass Spectrometry: A Powerful Tool for Merging Targeted and Non-targeted Metabolomics. Anal Chem 2017; 89(14):7667–74. https://doi.org/10.1021/acs.analchem.7b01624 PMID: 28581703

36. Agrawal S, Kumar S, Sehgal R, George S, Gupta R, Poddar S et al. El-MAVEN: A Fast, Robust, and User-Friendly Mass Spectrometry Data Processing Engine for Metabolomics. Methods Mol Biol 2019; 1978:301–21. https://doi.org/10.1007/978-1-4939-9236-2_19 PMID: 31119671

37. Chambers MC, Maclean B, Burke R, Amodei D, Ruderman DL, Neumann S et al. A cross-platform toolkit for mass spectrometry and proteomics. Nat Biotechnol 2012; 30(10):918–20. https://doi.org/10.1038/nbt.2377 PMID: 23051804

38. Heinrich P, Kohler C, Ellmann L, Kuerner P, Spang R, Oefner PJ et al. Correcting for natural isotope abundance and tracer impurity in MS-, MS/MS- and high-resolution-multiple-tracer-data from stable isotope labeling experiments with IsoCorrectoR. Sci Rep 2018; 8(1):17910. https://doi.org/10.1038/s41598-018-36293-4 PMID: 30559398